ADVANCED OPTICAL MATERIALS
www.advopticalmat.de

Photochromic Mechanism and Dual-Phase Formation in Oxygen-Containing Rare-Earth Hydride Thin Films

Marcus Hans, Tuan T. Tran, Sigurbjörn M. Aðalsteinsson, Dmitrii Moldarev, Marcos V. Moro, Max Wolff, and Daniel Primetzhofer*

The phase formation of a photochromic $Gd_{0.31}(H_{0.55}O_{0.45})_{0.69}$ thin film, grown by reactive magnetron sputtering, is critically evaluated. Oxygen is preferably incorporated into the underdense columnar grain boundaries, when the as-deposited gadolinium hydride film is exposed to ambient conditions. Two phases, Gd_2O_3 and GdH_2, are formed with significant compressive residual stress of 5.9 ± 1.5 GPa. These findings, extracted from transmission electron microscopy, X-ray diffraction and atom probe tomography, provide a straightforward explanation for the photochromic effect. The mechanism can be understood as photon-induced hydrogen transfer between the two phases, identical in nature to the photochromic effect in bulk yttrium hydride at high pressure.

1. Introduction

While the discovery of reversible photo-darkening in oxygen-containing yttrium hydride thin films opened up a new class of technologically relevant photochromic materials,[1] the underlying physical mechanism of the photochromic effect is still debated. These thin films were synthesized by reactive magnetron sputtering in hydrogen/argon atmosphere, oxygen was incorporated upon venting of the vacuum chamber subsequently to the thin film growth, and a face-centered cubic (fcc) crystal structure has been reported (space group $Fm\bar{3}m$, CaF_2 prototype).[1,2] The photochromic effect was also observed in oxygen-containing gadolinium, dysprosium as well as erbium hydride and it has been concluded that reactively sputtered lanthanide-based hydrides behave similarly as the yttrium-based thin films, suggesting a common physical mechanism of the photochromic effect.[3] Based on charge neutrality considerations, the authors suggested a single-phase structure and introduced the term "metal oxyhydrides,"[3] whereas previously such photochromic thin films were referred to as oxygen-containing metal hydrides.[1,2,4–7] The single-phase structure notion has been emphasized further by the proposal of a generalized simplified model of an anion-disordered fcc lattice.[8] This model was based on ion beam analysis and X-ray diffraction data, obtained from photochromic oxygen-containing scandium, yttrium, and gadolinium hydride thin films.[8] Recently, diffraction data from photochromic oxygen-containing yttrium hydride were interpreted as indication for a multiphase nature.[9] Despite the fact that the phase formation has not been identified,[9] the interpretation of a multiphase nature is obviously in conflict with the notion of single-phase photochromic metal oxyhydride thin films.[3,8] Here, we critically evaluate the phase formation of photochromic oxygen-containing gadolinium hydride thin films. The evidence of a dual-phase structure in combination with a significant compressive residual stress state provides a straightforward explanation for the photochromic effect. Consequently, the notion of single-phase photochromic metal oxyhydrides, discussed in literature, is flawed.

Dr. M. Hans
Materials Chemistry
RWTH Aachen University
Kopernikusstr. 10, Aachen D-52074, Germany
E-mail: hans@mch.rwth-aachen.de

Dr. T. T. Tran, S. M. Aðalsteinsson, D. Moldarev, Dr. M. V. Moro, Prof. M. Wolff, Prof. D. Primetzhofer
Department of Physics and Astronomy
Uppsala University
Lägerhyddsvägen 1, Uppsala S-75120, Sweden

D. Moldarev
Department of Materials Science
National Research Nuclear University MEPhI
Kashirskoe hwy 3, Moscow R-115409, Russia

The ORCID identification number(s) for the author(s) of this article can be found under https://doi.org/10.1002/adom.202000822.

DOI: 10.1002/adom.202000822

2. Evidence for Dual-Phase Formation

The average chemical composition of $Gd_{0.31}(H_{0.55}O_{0.45})_{0.69}$ was determined by means of multiple ion beam-based techniques as shown in **Figure 1**. In order to enhance the accuracy of the analysis, the set of spectra was evaluated following an iterative self-consistent approach.[10,11] Elastic backscattering spectrometry shows a rather homogeneous gadolinium concentration throughout the film. The depth profile from nuclear reaction analysis reveals that hydrogen is depleted to ≈16 at% in the near-surface region and is found otherwise between ≈36 and ≈44 at% (statistic uncertainty of ≈3 at%). These results are considered as boundary conditions in the coincidence time-of-flight

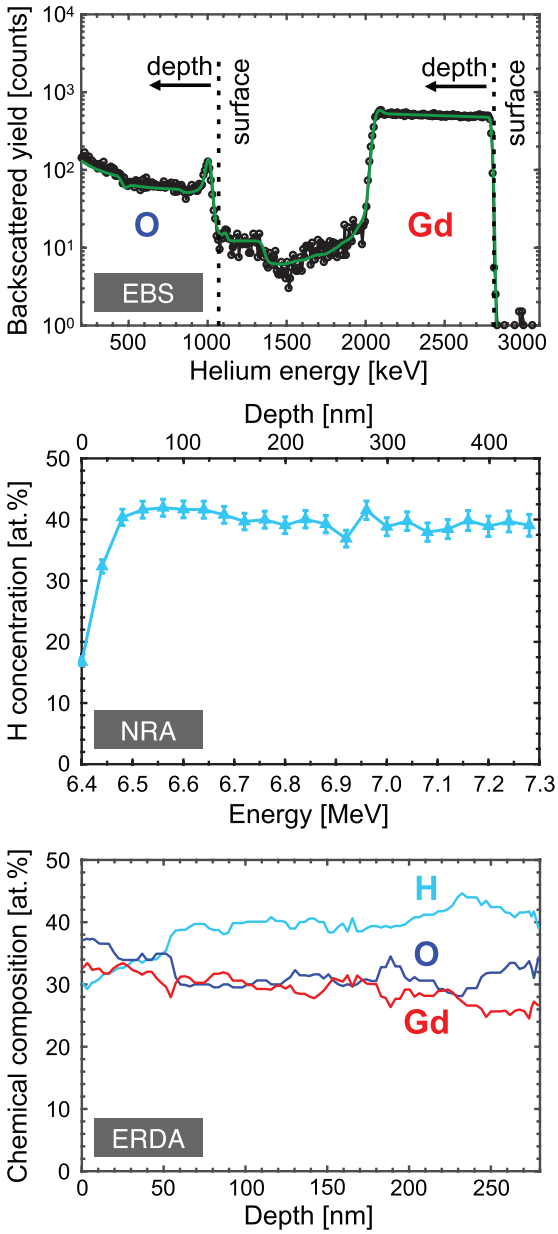

Figure 1. Ion beam analysis including elastic backscattering spectrometry (EBS), nuclear reaction analysis (NRA), and coincidence time-of-flight elastic recoil detection analysis (ERDA). Depth profile values in nanometers were calculated using the measured areal density as well as the film thickness.

elastic recoil detection analysis depth profile that exhibits a statistic uncertainty of 1 at%. It is evident that gadolinium, hydrogen, as well as oxygen concentrations vary approximately between 25 and 32 at%, 37 and 44 at%, as well as 28 and 34 at%, respectively (excluding the near-surface region). The photochromic response of a representative thin film, grown under similar conditions, after 5 min of illumination was ≈44% as shown in Figure S1, Supporting Information. The original transparent state was obtained after storage in the dark for 210 min. Photochromic response is here defined as the ratio of the averaged optical transmission contrast (previously calibrated to

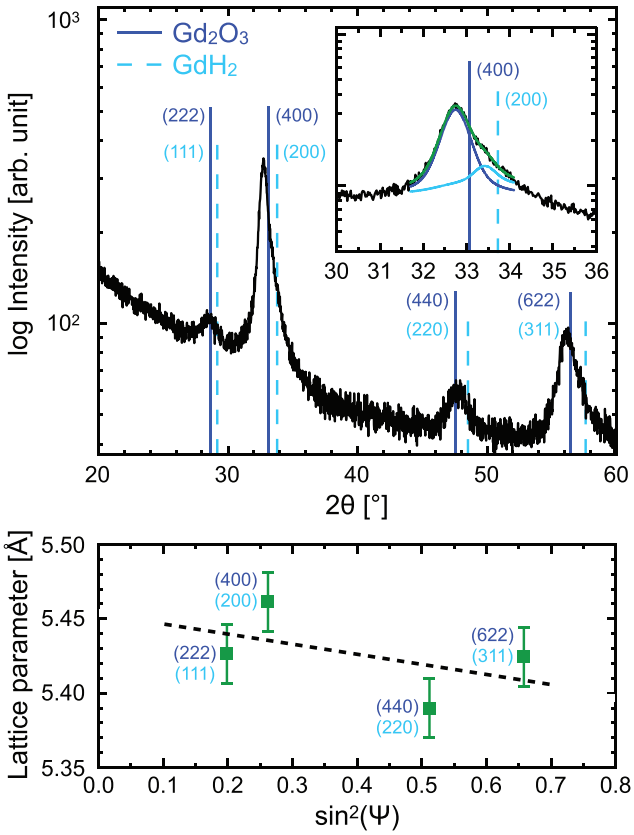

Figure 2. Phase formation and estimation of the residual stress state based on X-ray diffraction. Reference lines of Gd_2O_3 (space group $Ia\bar{3}$) and GdH_2 (space group $Fm\bar{3}m$) correspond to ICDD powder diffraction files 00-012-0797 and 00-050-1107, respectively.

100% transmission in air) of the spectra before and after illumination (integrated within the wavelength range from 500 to 900 nm) to the transmission before illumination. Further measurement details can be found in the Supporting Information. It should be noticed that in situ investigations by elastic recoil detection analysis during illumination of an oxygen-containing yttrium hydride thin film, causing photo-darkening in a high vacuum environment, showed no significant changes (≈1 at%) in the chemical composition.[11]

The phase formation and residual stress state were investigated by X-ray diffraction as presented in **Figure 2**. Diffraction peaks can be assigned to bixbyite Gd_2O_3 (space group $Ia\bar{3}$) and fcc GdH_2 (space group $Fm\bar{3}m$) phases that are crystallographically similar. The inset shows the peak originating from (400)/(200) lattice planes. It is evident that the diffraction peak is asymmetric and contributions of Gd_2O_3 as well as GdH_2 are revealed by using two pseudo-Voigt functions. The sum of both fits is in excellent agreement with the measured raw data. Hence, the diffraction data indicate the dual-phase formation of Gd_2O_3 and GdH_2 in the $Gd_{0.31}(H_{0.55}O_{0.45})_{0.69}$ thin film. The peak positions of the fits from Gd_2O_3 (400) and GdH_2 (200) lattice planes are 32.7° and 33.4° and corresponding full width at half maximum values are 0.7° and 0.9°, respectively. Therefore, the difference in peak positions of the two phases is on the same order as the peak width and the contributions of

Gd_2O_3 and GdH_2 cannot be unambiguously identified for broad diffraction peaks with low intensity, i.e., (222)/(111), (440)/(220), and (622/311).

A compressive residual stress of 5.9 ± 1.5 GPa was estimated based on $\sin^2\psi$ analysis in combination with the Seemann–Bohlin method.[12] A single pseudo-Voigt function was used for each diffraction peak and an elastic modulus of 113 GPa as well as Poisson's ratio of 0.27 from GdH_2 were assumed.[13] The uncertainty of lattice parameter values on the order of 0.02 Å was determined by comparison of the peak position obtained from the weighted contributions of Gd_2O_3 (400) and GdH_2 (200) with the single pseudo-Voigt peak position fit. Despite the relatively large uncertainty in the absolute stress value of 25%, a significant compressive residual stress state is evident.

As mentioned above, the dual-phase formation of Gd_2O_3 and GdH_2 cannot be unambiguously identified by diffraction data since the difference in peak positions is on the same order as the peak width. It has been recently demonstrated that spinodal decomposition of metastable vanadium aluminum nitride cannot be unraveled by diffraction data for similar reasons, but is only revealed by chemical composition characterization at the nanometer scale.[14] Consequently, the notion of dual-phase formation of $Gd_{0.31}(H_{0.55}O_{0.45})_{0.69}$ is addressed by nanometer-scale characterization employing transmission electron microscopy and atom probe tomography in the following.

High-angle annular dark-field images of the $Gd_{0.31}(H_{0.55}O_{0.45})_{0.69}$ thin film are shown in **Figure 3**. The cross-section reveals a film thickness of ≈1.3 µm. From the combination of the film thickness with the areal density, measured by ion beam analysis, a density of 6.6 g cm^{-3} is obtained for $Gd_{0.31}(H_{0.55}O_{0.45})_{0.69}$ that is 3% lower than the reported density of $Gd_{0.36}(H_{0.26}O_{0.74})_{0.64}$.[15] Moreover, a fine-grained structure is formed within the initial growth stages of the magnetron sputtered thin film which evolves into a columnar growth morphology.[16] Plane-view images were taken from a lamella extracted approximately at half of the film thickness and reveal column diameters on the order of 40–60 nm. Since the high-angle annular dark-field signal is related to the atomic number, the contrast differences reveal that the columnar grain boundary regions exhibit a significantly different chemical composition than the grains. Energy-dispersive X-ray spectroscopy mapping demonstrates enhanced presence of oxygen in the grain boundary regions. It is well known that low-energy ion irradiation results in the formation of an underdense microstructure.[16] Therefore, it can be rationalized that oxygen is preferably incorporated into the underdense columnar grain boundaries, when the as-deposited gadolinium hydride film is exposed to ambient conditions. Substantial oxygen uptake can be understood by the large thermodynamic driving force for substitution of hydrogen by oxygen.[15] It may be speculated that the significant compressive residual stress state is induced by oxygen incorporation upon exposure to the ambient. The microstructure of $Gd_{0.31}(H_{0.55}O_{0.45})_{0.69}$ is very similar to a photochromic $Y_{0.33}(H_{0.42}O_{0.58})_{0.67}$ thin film and the comparison is presented in Figure S2, Supporting Information.

The chemical composition at the nanometer scale was quantified by atom probe tomography. This technique combines time-of-flight mass spectrometry with projection microscopy of field-evaporated atoms and enables imaging

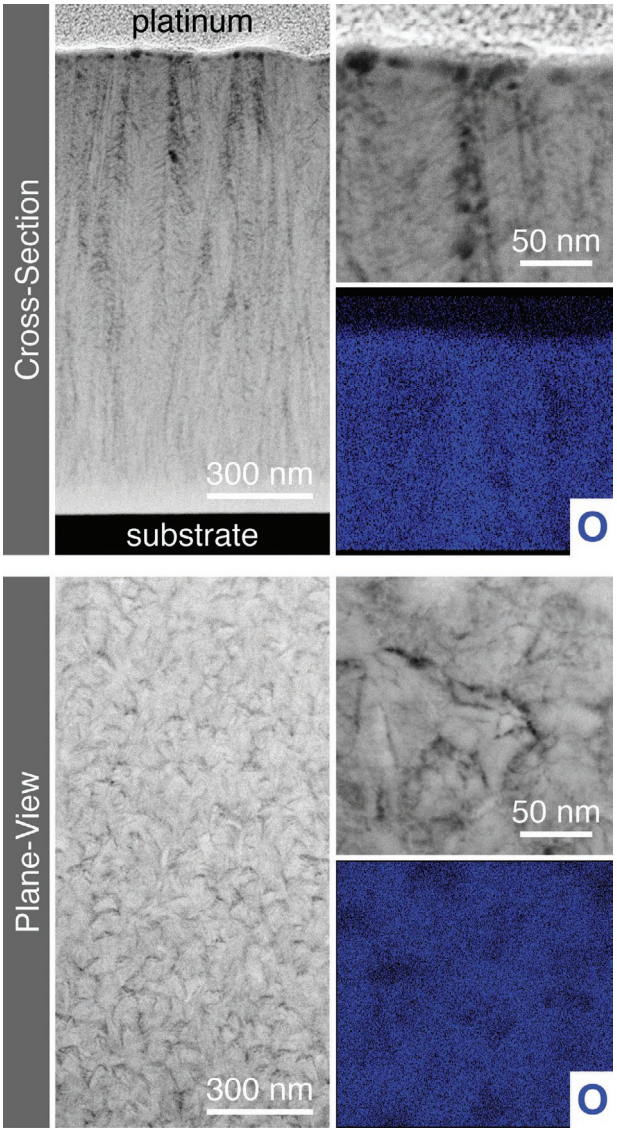

Figure 3. High-angle annular dark-field images of a cross-section and a plane-view thin film lamella. The regions of the oxygen concentration signal correspond to the high-magnification micrographs.

of hydrogen.[17–20] Reconstructions of gadolinium together with hydrogen as well as gadolinium together with oxygen atomic positions are shown in **Figure 4**. While gadolinium atoms can be observed across the whole reconstruction, it is evident that hydrogen and oxygen exhibit an anti-correlation since hydrogen-rich regions are deficient in oxygen and vice versa. The near-surface region shows an enrichment in oxygen and the reduced hydrogen composition range of 6–14 at% is in agreement with the observations from the nuclear reaction analysis depth profile (Figure 1). Impurities of 1 at% carbon as well as <1 at% gallium were found to be homogeneously distributed and originate from the growth process as well as the atom probe specimen preparation, respectively. The complex mass spectrum and reconstructions of GdH and GdO molecular ions can be found in Figures S3 and S4, Supporting Information, respectively.

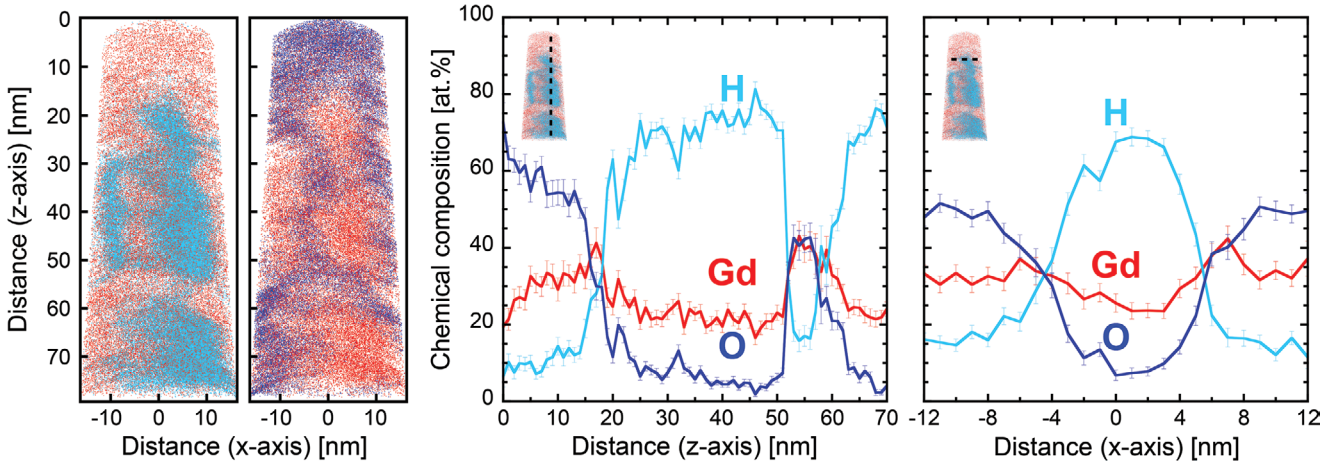

Figure 4. Atom probe tomography reconstructions of gadolinium (red), hydrogen (cyan), and oxygen (blue). Vertical (in growth direction) and horizontal (perpendicular to growth direction) chemical composition profiles were obtained from the regions indicated by dashed lines.

Quantitative chemical composition information is obtained from depth profiles that are also provided in Figure 4. The amount of gadolinium varies between 17 and 27 at% in the hydrogen-rich regions and between 30 and 35 at% in the oxygen-rich regions, while 33 at% would be expected for GdH_2 and 40 at% for Gd_2O_3. However, the absolute chemical compositions measured by laser-assisted atom probe tomography are significantly affected by the evaporation conditions. Laser-assisted field evaporation of titanium deuteride with a laser pulse energy of 10 pJ (identical energy as in the present work) revealed that the measured titanium content was reduced down to 27 at% instead of the expected 33–35 at% and explained by an increased fraction of background counts caused by significant DC evaporation.[21] The mass spectrum, shown in Figure S3, Supporting Information, also reveals a relatively high fraction of background counts and it appears reasonable to assume that the absolute gadolinium composition is therefore underestimated. Moreover, the mass spectrum exhibits mostly molecular ions and it has been demonstrated that the relative amounts depend significantly on the electrostatic field.[22] Furthermore, the hydrogen composition is usually overestimated by laser-assisted atom probe tomography due to the presence of residual gas. In order to reduce the influence of residual hydrogen from the ultra-high vacuum chamber, the electrostatic field should be maximized,[22] which is in line with the employment of a relatively low laser pulse energy of 10 pJ. Despite all of the discussed challenges with respect to hydrogen quantification by laser-assisted atom probe tomography, the combination of diffraction and microstructure data, Figures 2 and 3, with spatially resolved composition analysis at the nanometer scale supports the dual-phase formation of Gd_2O_3 and GdH_2. It should be noticed that these phases may contain up to 10 at% of solute hydrogen and oxygen, respectively.

3. Implications for the Photochromic Mechanism

In the following, the physical mechanism for the photochromic effect in oxygen-containing rare-earth hydride thin films is discussed. Photochromism in metal hydrides was first reported for an yttrium foil that was pressurized in hydrogen to 5.8 GPa.[23] The phase formation of fcc YH_2 and hexagonal YH_3 (space group $P\bar{3}c1$) was demonstrated and it was suggested that infrared laser illumination causes hydrogen transfer from hexagonal YH_3 to the fcc YH_2.[23] This argument was based on the optical response of YH_x thin films upon hydrogen loading: starting from a transmittance of 0.008 at $x = 1.9$, a transmittance minimum of <0.002 was obtained at $x = 2.1$, and coexistence of fcc $YH_{2.1}$ as well as the hexagonal phase was observed for $x > 2.1$.[24] In good agreement with these data, hydrogen uptake of $\Delta x = 0.22$ was estimated by Ohmura et al. from the measured contraction of the fcc YH_2 lattice upon photodarkening.[23] Hence, it can be learned that prerequisites for photochromism in bulk yttrium hydride at room temperature are the coexistence of two phases as well as a high pressure, i.e., 5.8 GPa.

The here presented data provide evidence for the coexistence of fcc GdH_2 as well as bixbyite Gd_2O_3 in photochromic $Gd_{0.31}(H_{0.55}O_{0.45})_{0.69}$ and a compressive residual stress on the order of 5.9 ± 1.5 GPa was estimated. Since the dual-phase structure as well as the significant compressive stress state are in agreement with prerequisites for photochromism in YH_x,[23] we propose a mechanism of photon-induced hydrogen transfer from the hydrogen-containing bixbyite Gd_2O_3 to the fcc GdH_2 phase, concomitantly causing the photo-darkening. As mentioned above, the microstructures of magnetron sputtered $Gd_{0.31}(H_{0.55}O_{0.45})_{0.69}$ and $Y_{0.33}(H_{0.42}O_{0.58})_{0.67}$ are very similar (Figure S2, Supporting Information). Based on the contrast differences at the columnar grain boundaries in both material systems, it can be learned that the dual-phase formation is not limited to $Gd_{0.31}(H_{0.55}O_{0.45})_{0.69}$ and appears to be relevant for photochromic oxygen containing rare-earth hydride thin films. A change in relative intensities of the hydride and oxide contributions due to hydrogen transfer could also explain the observed peak shift in oxygen-containing yttrium hydride that was interpreted as a contraction of the single-phase fcc lattice.[4] It has to be emphasized that the dual-phase formation identified here clearly speaks against the notion of an oxyhydride nature of such photochromic thin films and charge neutrality arguments cannot be based on a formal metal valence of +3.[3,8]

While the measured compressive residual stress state of 5.9 ± 1.5 GPa in $Gd_{0.31}(H_{0.55}O_{0.45})_{0.69}$ is in very good agreement with the pressure for bulk photochromic yttrium hydride,[23] the stress distribution along the film thickness remains unclear. The fine-grained structure within the initial growth stages of the thin film, Figure 3, exhibits a large volume fraction of grain boundaries. For chromium and chromium nitride thin films it has been discussed that a large volume fraction of grain boundaries is responsible for ion irradiation-induced formation of compressive stresses. [25] As a result the photochromic effect of oxygen-containing rare-earth hydride thin films could be confined to a region close to the interface between thin film and substrate which should be characterized by the largest compressive residual stress state.

4. Conclusions

A photochromic oxygen-containing gadolinium hydride thin film with an average composition of $Gd_{0.31}(H_{0.55}O_{0.45})_{0.69}$ was grown by reactive magnetron sputtering. Transmission electron microscopy data revealed that oxygen is preferably incorporated into the underdense columnar grain boundaries, when the as-deposited gadolinium hydride film is exposed to ambient conditions. Structural characterization by X-ray diffraction in combination with spatially resolved composition analysis at the nanometer scale by atom probe tomography supports the dual-phase formation of Gd_2O_3 and GdH_2. Moreover, the dual-phase formation is accompanied by a significant compressive residual stress of 5.9 ± 1.5 GPa. Since the formation of two phases as well as the significant compressive stress state is in agreement with prerequisites for photochromism in bulk yttrium hydride at high pressure, the photochromic mechanism can be understood as photon-induced hydrogen transfer between the two phases. As the microstructures of photochromic $Gd_{0.31}(H_{0.55}O_{0.45})_{0.69}$ and photochromic $Y_{0.33}(H_{0.42}O_{0.58})_{0.67}$ are very similar, it can be learned that the dual-phase formation is not limited to $Gd_{0.31}(H_{0.55}O_{0.45})_{0.69}$ and appears to be relevant for photochromic oxygen-containing rare-earth hydride thin films.

5. Experimental Section

Synthesis: Thin film growth was carried out by reactive direct current magnetron sputtering in a Balzers Union system and the base pressure was $<7 \times 10^{-3}$ Pa. The Gd target (99.9% nominal purity, 54 mm diameter, 1 mm thickness) was separated by 6.5 cm from the electrically grounded soda-lime substrate. The discharge was operated for 30 min at a current of 120 mA without intentional heating of the substrate. The deposition pressure was 0.9 Pa with the H_2/Ar partial pressure ratio of 0.01. Subsequent to the deposition, the thin film was exposed to ambient conditions.

Characterization: The chemical composition was investigated by ion beam analysis using the 5-MV NEC-5SDH-2 tandem accelerator at Uppsala University.[26] 3.1 MeV He^+ primary ions were used for elastic backscattering spectrometry and hydrogen depth profiles were obtained via the resonant $^1H(^{15}N,\alpha\gamma)^{12}C$ nuclear reaction using a $^{15}N^{2+}$ primary beam. Data analysis was done with SIMNRA.[27] Coincidence time-of-flight elastic recoil detection analysis was employed using 36 MeV I^{8+} primary ions. Quantitative depth profiles of the elemental composition were obtained using the analysis software Potku.[28]

The phase formation was studied by X-ray diffraction using a Siemens D5000 diffractometer with a Goebel mirror. The incidence angle of the Cu Kα source was fixed at 2° and voltage and current were set at 45 kV and 40 mA, respectively.

Microstructural characterization of thin lamellae was employed by scanning transmission electron microscopy using a FEI Titan Themis 200 at 200 kV. High-angle annular dark-field images were acquired and the local chemical composition distribution was qualitatively investigated by energy-dispersive X-ray spectroscopy mapping with a SuperX detector.

The spatially resolved chemical composition at the nanometer scale was quantitatively characterized by atom probe tomography. Field evaporation of a needle-shape specimen was assisted by laser pulsing in a CAMECA local electrode atom probe 4000X HR. A total of 1.5 million ions were collected at laser pulse energy, pulse frequency, base temperature, and detection rate of 10 pJ, 125 kHz, 30 K, and 0.5%, respectively.

Thin lamellae and needle-shape specimens were prepared by focused ion beam techniques in a FEI Helios NanoLab 660 dual-beam microscope using Ga ions.

Supporting Information

Supporting Information is available from the Wiley Online Library or from the author.

Acknowledgements

The authors would like to thank Dr. Ayan Samanta for access to the spectrophotometer at the Department of Chemistry at Uppsala University. Accelerator operation was supported by the Swedish Research Council VR-RFI (contracts no. 821-2012-5144 and no. 2017-00646_9) and the Swedish Foundation for Strategic Research (contract RIF14-0053).

Conflict of Interest

The authors declare no conflict of interest.

Keywords

atom probe tomography, ion beam analysis, magnetron sputtering, photochromism

Received: May 18, 2020
Revised: June 17, 2020
Published online:

[1] T. Mongstad, C. Platzer-Björkman, J. P. Maehlen, L. P. A. Mooij, Y. Pivak, B. Dam, E. S. Marstein, B. C. Hauback, S. Z. Karazhanov, *Sol. Energy Mater. Sol. Cells* **2011**, *95*, 3596.
[2] T. Mongstad, C. Platzer-Björkman, S. Z. Karazhanov, A. Holt, J. P. Maehlen, B. C. Hauback, *J. Alloys Compd.* **2011**, *509*, S812.
[3] F. Nafezarefi, H. Schreuders, B. Dam, S. Cornelius, *Appl. Phys. Lett.* **2017**, *111*, 103903.
[4] J. P. Maehlen, T. Mongstad, C. C. You, S. Z. Karazhanov, *J. Alloys Compd.* **2013**, *580*, S119.
[5] C. V. Chandran, H. Schreuders, B. Dam, J. W. G. Janssen, J. Bart, A. P. M. Kentgens, P. J. M. van Bentum, *J. Phys. Chem. C* **2014**, *118*, 22935.

[6] C. C. You, D. Moldarev, T. Mongstad, D. Primetzhofer, M. Wolff, E. S. Marstein, S. Z. Karazhanov, *Sol. Energy Mater. Sol. Cells* **2017**, *166*, 185.
[7] J. Montero, F. A. Martinsen, M. García-Tecedor, S. Z. Karazhanov, D. Maestre, B. C. Hauback, E. S. Marstein, *Phys. Rev. B* **2017**, *95*, 201301(R).
[8] S. Cornelius, G. Colombi, F. Nafezarefi, H. Schreuders, R. Heller, F. Munnik, B. Dam, *J. Phys. Chem. Lett.* **2019**, *10*, 1342.
[9] E. M. Baba, J. Montero, E. Strugovshchikov, E. Ö. Zayim, S. Z. Karazhanov, *Phys. Rev. Mater.* **2020**, *4*, 025201.
[10] M. V. Moro, R. Holeňak, L. Zendejas Medina, U. Jansson, D. Primetzhofer, *Thin Solid Films* **2019**, *686*, 137416.
[11] M. V. Moro, D. Moldarev, C. C. You, E. M. Baba, S. Z. Karazhanov, M. Wolff, D. Primetzhofer, *Sol. Energy Mater. Sol. Cells* **2019**, *201*, 110119.
[12] V. Valdova, R. Kužel Jr., R. Černý, D. Rafaja, J. Musil, S. Kadlec, A. J. Perry, *Thin Solid Films* **1990**, *193–194*, 401.
[13] G. S. Priyanga, R. Rajeswarapalanichamy, K. Iyakutti, *Mater. Sci. Semicond. Process.* **2015**, *31*, 415.
[14] M. Hans, H. Rueß, Z. Czigány, J. Krause, P. Ondračka, D. Music, S. Evertz, D. M. Holzapfel, D. Primetzhofer, J. M. Schneider, *Surf. Coat. Technol.* **2020**, *389*, 125641.
[15] A. Miniotas, B. Hjörvarsson, L. Douysset, P. Nostell, *Appl. Phys. Lett.* **2000**, *76*, 2056.
[16] I. Petrov, P. B. Barna, L. Hultman, J. E. Greene, *J. Vac. Sci. Technol., A* **2003**, *21*, S117.
[17] R. Gemma, T. Al-Kassab, R. Kirchheim, A. Pundt, *Scr. Mater.* **2012**, *67*, 903.
[18] D. Haley, P. A. J. Bagot, M. P. Moody, *Microsc. Microanal.* **2017**, *23*, 307.
[19] Y. Chang, W. Lu, J. Guénolé, L. T. Stephenson, A. Szczpaniak, P. Kontis, A. K. Ackerman, F. F. Dear, I. Mouton, X. Zhong, S. Zhang, D. Dye, C. H. Liebscher, D. Ponge, S. Korte-Kerzel, D. Raabe, B. Gault, *Nat. Commun.* **2019**, *10*, 942.
[20] Y.-S. Chen, P. A. J. Bagot, M. P. Moody, D. Haley, *Int. J. Hydrogen Energy* **2019**, *44*, 32280.
[21] Y. H. Chang, I. Mouton, L. T. Stephenson, M. Ashton, G. K. Zhang, A. Szczpaniak, W. J. Lu, D. Ponge, D. Raabe, B. Gault, *New J. Phys.* **2019**, *21*, 053025.
[22] I. Mouton, A. J. Breen, S. Wang, Y. Chang, A. Szczepaniak, P. Kontis, L. T. Stephenson, D. Raabe, M. Herbig, T. B. Britton, B. Gault, *Microsc. Microanal.* **2019**, *25*, 481.
[23] A. Ohmura, A. Machida, T. Watanuki, K. Aoki, S. Nakano, K. Takemura, *Appl. Phys. Lett.* **2007**, *91*, 151904.
[24] A. Remhof, J. W. J. Kerssemakers, S. J. van der Molen, R. Griessen, E. S. Kooji, *Phys. Rev. B* **2002**, *65*, 054110.
[25] R. Daniel, D. Holec, M. Bartosik, J. Keckes, C. Mitterer, *Acta Mater.* **2011**, *59*, 6631.
[26] M. Mayer, S. Möller, M. Rubel, A. Widdowson, S. Charisopoulos, T. Ahlgren, E. Alves, G. Apostolopoulos, N. P. Barradas, S. Donnelly, S. Fazinić, K. Heinola, O. Kakuee, H. Khodja, A. Kimura, A. Lagoyannis, M. Li, S. Markelj, M. Mudrinic, P. Petersson, I. Portnykh, D. Primetzhofer, P. Reichart, D. Ridikas, T. Silva, S. M. Gonzalez de Vicente, Y. Q. Wang, *Nucl. Fusion* **2020**, *60*, 025001.
[27] M. Mayer, W. Eckstein, H. Langhuth, F. Schiettekatte, U. von Toussaint, *Nucl. Instrum. Methods Phys. Res., Sect. B* **2011**, *269*, 3006.
[28] K. Arstila, J. Julin, M. I. Laitinen, J. Aalto, T. Konu, S. Kärkkäinen, S. Rahkonen, M. Raunio, J. Itkonen, J.-P. Santanen, T. Tuovinen, T. Sajavaara, *Nucl. Instrum. Methods Phys. Res., Sect. B* **2014**, *331*, 34.